Influence of substrate characteristics on single Ti splat bonding to ceramic substrates by cold spray

Sara I. Imbriglio[1] · Nicolas Brodusch[1] · Maniya Aghasibeig[2] · Raynald Gauvin[1] · Richard R. Chromik[1,*]

[1] Department of Mining and Materials Engineering, McGill University, 3610 University Street, Montreal, QC H3A 0C5

[2] National Research Council Canada, Boucherville, QC, J4B 6Y4, Canada

* Corresponding author. Telephone: +1(514) 398-5686; Fax: +1 (514) 398-4492

Email address: richard.chromik@mcgill.ca

Abstract The cold spray technique may be used to fabricate metal matrix composites and to metallize ceramics. Both applications involve the creation of metal/ceramic interfaces, which are well researched for other processes but not nearly as much for cold spray. Here, the effect of ceramic substrate composition and surface roughness on adhesion strength of metallic splats is investigated. Splat adhesion testing was performed on Ti splats deposited on Al_2O_3 substrates with varying average reduced peak height roughness (R_{pk}) values. Ti splats sprayed onto Al_2O_3 with the lowest surface roughness had a higher bond strength (305 ± 87 MPa) than splats deposited on the higher surface roughness Al_2O_3 (237 ± 47 MPa). Failed interfaces revealed that the bonding mechanism for substrates with higher surface roughness is predominantly mechanical interlocking. Adhesion to the Al_2O_3 substrate with low surface roughness is predominantly along the periphery of the particle where jetting occurs. Splat adhesion testing was also performed on Ti splats deposited on SiC. Ti splats had a significantly higher bond strength to all Al_2O_3 substrates than to

SiC. Post-test observations of SiC substrates showed little evidence of bonding. Several rebounded or detached splats left traces of Ti along the periphery of the impacted particle.

Keywords titanium · alumina · silicon carbide · cold spray · interface · adhesion

1. Introduction

High pressure cold spray is a coating deposition technique by which powder is fed into a heated high-pressure gas flow and accelerated to supersonic velocities by a de Laval nozzle. The powders, accelerated to high velocity, impact on a substrate and if bonded create a 'splat'. The gas temperature is maintained below the melting temperature of the powder (Ref 1, 2). Thus, for metal/metal interfaces, solid-state bonding between the powder and substrate occurs by extreme plastic deformation and the formation of adiabatic shear instabilities (ASI). Mechanical clamping and metallurgical bonding are reported for these interfaces (Ref 3, 4, 5). While a significant amount of work has been done to understand adhesion in metal/metal interfaces by cold spray, metal/ceramic interfaces are not well understood given the low deformability of the ceramic (Ref 6, 7, 8).

Two types of metal/ceramic interfaces created by cold spray are addressed in the literature. Metal matrix composites (MMC) with ceramic reinforcements have been deposited to improve adhesion, increase hardness, reduce porosity and improve tribological properties, among other advantages (Ref 2, 6, 9). Ceramic metallization by cold spray is investigated for various applications such as in the electronics industries (Ref 10, 11, 12, 13). These coatings can also be interesting for the

biomedical industry as Ti coatings on Al_2O_3 orthopedic implants can be specially engineered to counter issues involving the low toughness of the ceramic (Ref 14, 15).

In the deposition of MMCs, it is generally agreed that ceramic particles are embedded in coatings by the deforming metal phase with no chemical interaction (Ref 2, 7, 16). However, for metallic coatings deposited on ceramic substrates, the bonding mechanism cannot be solely attributed to mechanical clamping. Strong bonds are observed between Ti and Al coatings deposited on atomically smooth Al_2O_3 in addition to Al coatings deposited on AlN substrates (Ref 13, 17, 18). Local hetero-epitaxy was concluded to play a role in bonding between these heterogeneous materials. The kinetic energy of splats is converted to heat during plastic deformation, leading to increased atomic mobility and potential for hetero-epitaxial growth (Ref 13, 17, 18, 19). Atomic mobility and intermixing of atoms at the interface has also been attributed to amorphisation at the interface during plastic deformation (Ref 20). Increased substrate temperature has been found to increase adhesion strength in metal/ceramic interfaces as it reportedly allows for a stronger chemical bond (Ref 10, 11, 18, 19, 21). However, while adhesion strength varies for different types of ceramics, the influencing parameters have not been fully identified. Drehmann et al. showed that traditional trends observed between bond strength and ionicity when wetting ceramics by metals are not respected in cold spray (Ref 18). Also, the coefficient of thermal expansion mismatch was not found to directly influence bond strength. Rather, a higher thermal conductivity and thermal effusivity of the substrate was assumed to have a positive effect as the interface contact temperature is lower. With a lower contact temperature, negative effects induced by the coefficient of thermal expansion mismatch between the metal and ceramic and tensile residual stresses are reduced (Ref 22). It is still unclear how substrate surface roughness will influence the chemical interaction in these metal/ceramic interfaces as mechanical clamping can also occur and if strong

bonds are formed at a single site of impact or if adhesion is promoted by further compaction from the impact of succeeding splats. On the one hand, cross-sectional micrographs have shown gapping in the interface of Al single splats deposited on APS-sprayed Al_2O_3 substrates but full Al coatings on sintered Al_2O_3 appeared continuous (Ref 19). On the other hand, Ti single splat deposited on zirconia only showed gaping near the center of the particle and bonding near the edge (Ref 23).

In this work, single splats of Ti are deposited on Al_2O_3 and SiC substrates. Ti has previously shown promising dense coatings with good adhesion to Al_2O_3 deeming further investigation (Ref 17). The ceramics were selected as they are commonly found in MMCs (Ref 6, 7, 24, 25, 26). The effect of substrate composition on adhesion strength is addressed and the influence of surface roughness on adhesion in the Ti/Al_2O_3 interface is investigated.

To measure bond strength, a splat adhesion test is used. This test, also referred to as a modified ball bond shear test, was introduced by Chromik et al. and later used by Goldbaum et al. (Ref 27, 28). Traditional testing techniques, such as DIN EN 582 or ASTM C-633-99, focus on full coating adhesion (Ref 19, 27). The splat adhesion test was designed for analysis of bonding at the first site of impact in the splat/substrate interface. By splat adhesion testing, significantly less material is used and fracture of the ceramic as well as the epoxy under tension is avoided (Ref 27, 28). Following splat adhesion testing, the failed interface was analysed through light microscopy and scanning electron microscopy (SEM) to understand the bonding mechanism and the influence of the ceramic surface characteristics. Splat/substrate cross-sections were also studied to understand the interface morphology and bond formation.

2. Experimental Procedure

Single splats of spherical, commercially pure, Ti (Grade 1, AP&C, Quebec, Canada) were deposited onto high purity sintered Al_2O_3 and SiC (AD-995, SC-30, CoorsTeK, Arkansas, USA) substrates. The CP-Ti powder has a size distribution of 0 to 45 μm. Figure 1(a) and (b) show the powder size distribution and morphology. By laser diffraction particle size analysis (LA-920, Horiba, Kyoto, Japan), the mean particle size is 29 μm. The Ti powder is dense with a martensitic microstructure as shown through electron channelling contrasts (ECC) (Fig. 1 (c)).

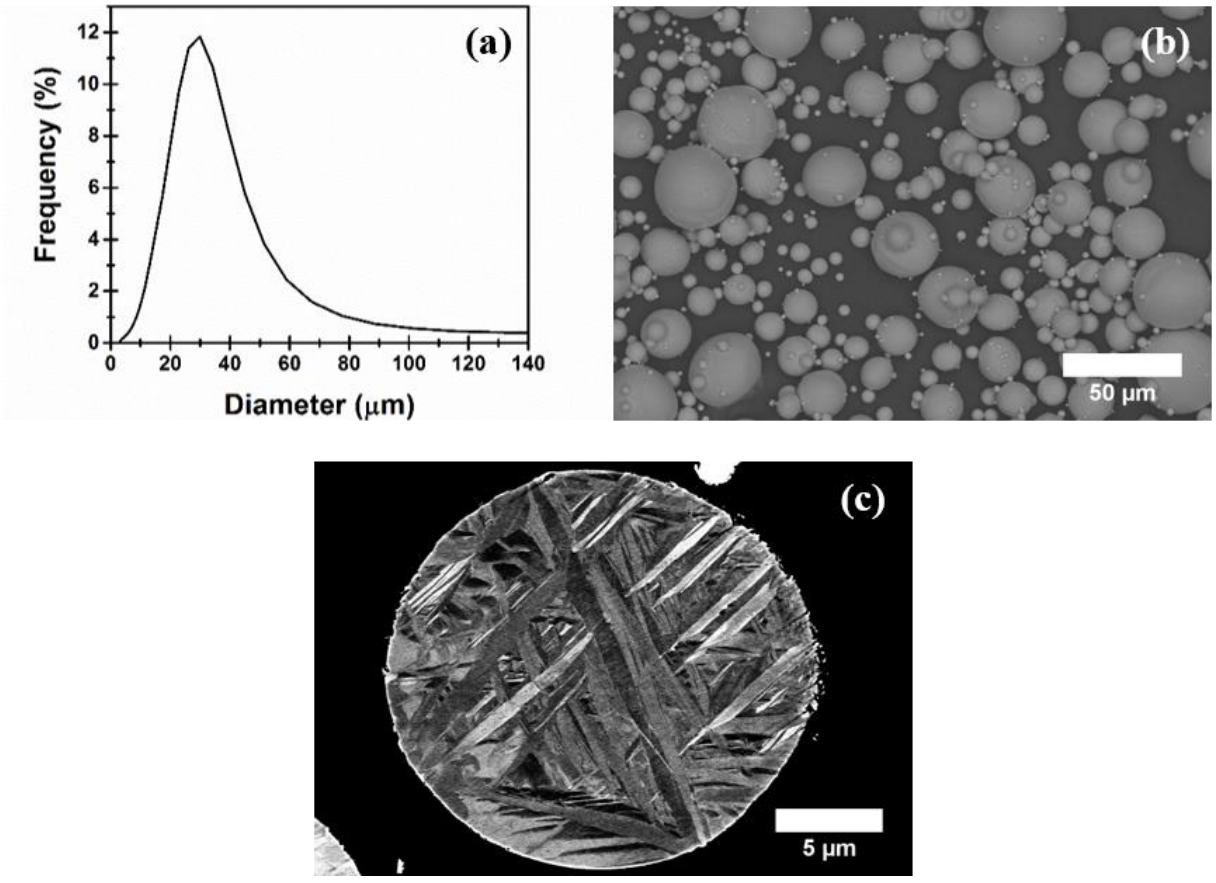

Fig. 1 The (a) powder size distribution, (b) powder morphology and (c) microstructure of the Ti powder.

The polycrystalline and sintered Al_2O_3 and SiC substrates had a thickness of approximately 12.7 mm. Figure 2 shows the as-received surface morphology of the substrates. Both substrates have a significant variation in grain size and grain morphology. The grains used in the sintering of SiC substrates are mostly smaller than those used to produce the Al_2O_3 substrates. Data from the manufacturer showed an average crystal size of 6 μm for the Al_2O_3 and 3 to 10 μm for the SiC samples.

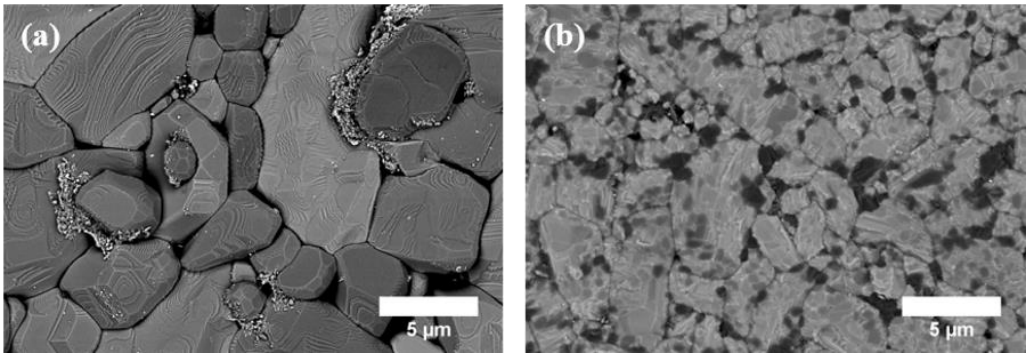

Fig. 2 A representative backscattered SEM image of the morphology and grain size of the as-received (a) Al_2O_3 and (b) SiC substrates

The chemistry of the substrates was characterised through energy-dispersive X-ray spectroscopy (EDS) in the SEM (SU-8230, Hitachi, Tokyo, Japan). Charging effects were reduced by using low accelerating voltages of 3 to 5 kV. A 3D Optical Surface Profiler (ZYGO, Connecticut, USA) was also used to measure surface roughness on 3x3 mm^2 and 87x87 μm^2 surface areas. Measurements were taken at two magnifications to determine the average roughness of the substrates and the local roughness at a length scale more similar to the size of a single splat. The reduced peak height value (R_{pk}) was used to characterize surface roughness as it is a better measure for sintered materials than R_a or R_k to reduce the effect of porosity. R_{pk} is the average height of peaks above the height of the core surface (R_k value) (Ref 29). Twelve areas on three as-received Al_2O_3 and SiC substrates were analysed to determine the average surface roughness of the substrates used.

Given a relatively high surface roughness of Al_2O_3 in comparison to SiC (Table 1), six halves of the Al_2O_3 substrates were polished to a final step of 60 μm diamond grinding disk and the other six halves were polished to a final step of 1 μm diamond suspension. Twelve areas on the six grinded and polished substrates were analysed to obtain the average R_{pk} value for these processed substrates. Average R_{pk} values measured by optical profilometry and sample identification used in the following sections of this work are shown in Table 1.

Table 1 Sample Roughness and Identification

Sample	R_{pk}, μm	Identification
As-received Al_2O_3	0.78 ± 0.38	Al_2O_3 (0.78)
60 μm diamond grinding of Al_2O_3	0.33 ± 0.07	Al_2O_3 (0.33)
1 μm diamond suspension polishing of Al_2O_3	0.16 ± 0.03	Al_2O_3 (0.16)
As-received SiC	0.39 ± 0.06	SiC

The Ti powder was deposited on both ceramics by cold spray (PCS-800, Plasma Giken, Saitama, Japan). Nitrogen was used as the carrier gas with a pressure of 4 MPa and a temperature of 800 °C. To deposit scattered single splats, the gun traverse speed was 1 m/s. The standoff distance was set to 30 mm. Once the feed rate was stable, the powder feeder was shut before scanning the surface of the substrate by the cold spray gun mounted on a robotic arm. As a result, only the powder that remained in the gas stream was available for deposition. This was done to ensure a population of splats that was appropriate for splat adhesion testing. Splats must be sufficiently far from one another in order to scratch single splats during splat adhesion testing.

Splat adhesion testing was conducted using a Micro-Combi Scratch Tester (CSM Instruments, Inc, Massachusetts, USA) in accordance with the testing methodology described by Chromik et al. and

Goldbaum et al. (Ref 27, 28). In this test, the flat face of a semi-circular stylus, 100 μm long, is used to shear single splats (Fig. 3). A normal force between 30 and 100 mN is applied to maintain contact between the stylus and the substrate. In a small number of tests, the stylus traveled fully or partially above the splat and these tests were disregarded in the analysis. A scratch length of 130 μm or 100 μm was used depending on the available space between splats. The splat is positioned approximately at the center of the scratch length. The scratch speed was set to 150 μm/min.

The splat adhesion test outputs a plot of tangential force applied on the stylus with respect to the scratch length. Baseline tangential force due to friction along the substrate and a peak tangential force due to the removal of the splat are recorded. Some Ti splats deposited on SiC rendered no distinguishable peak. A schematic of the test and an example plot of a test with a peak and one with no distinguishable peak are shown in Fig. 3.

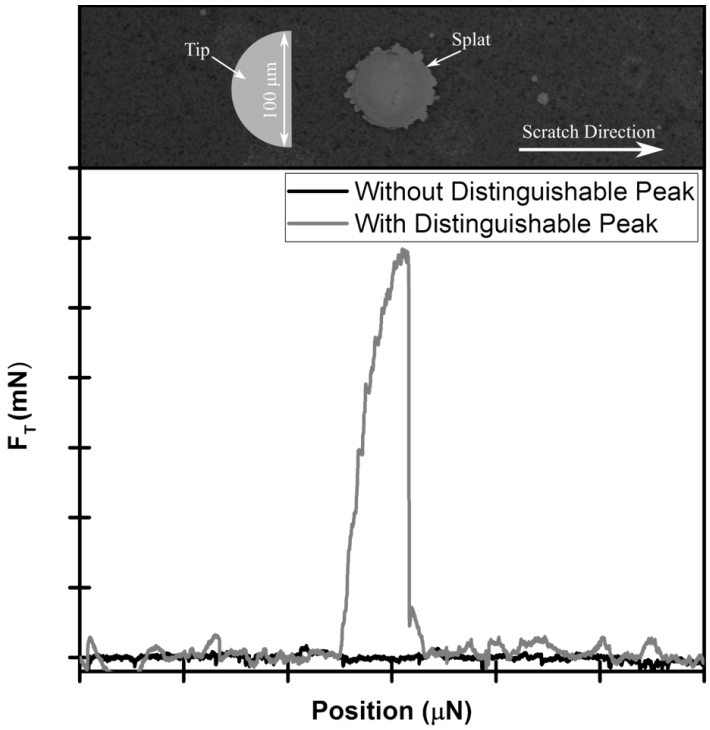

Fig. 3 Schematic of the splat adhesion test and output graph. The output graph shows a typical tangential force versus position graph with and without distinguishable peak

To process the splat adhesion test data, the baseline tangential force is subtracted from the peak.

The baseline was subtracted in OriginLab using the 2nd derivative method and fit with a spline.

Adhesion strength is then measured by Eq 1 (Ref 27, 28).

$$Adhesion\ Strength\ [MPa] = \frac{F_{T\ Peak}\ [mN] - F_{T\ Baseline}[mN]}{Projected\ Splat\ Area\ [\mu m^2]} * 1000 \quad \text{(Eq 1)}$$

where the projected splat area can be measured by Eq 2.

$$Projected\ Splat\ Area\ [\mu m^2] = \pi \left(\frac{w\ [\mu m]}{2}\right)^2 \quad \text{(Eq 2)}$$

where w is the splat diameter measured using the light optical microscope (LOM) on the scratch tester prior to testing.

To determine the approximate equivalent powder diameter prior to deposition, Eq 3 is used (Ref 28, 30). FR is the flattening ratio which can be calculated by dividing the diameter of the splat by its height (Ref 28). The height of the splat is measured by subtracting the height of the microscope when focusing on the substrate from the height of the microscope when focusing on the top of the splat (Ref 27, 28).

$$d[\mu m] = \left(\frac{w^3}{FR}\right)^{\frac{1}{3}} \quad \text{(Eq 3)}$$

At least 35 splats were tested for each material combination studied over a wide range of powder sizes. To compare the effect of surface roughness and composition on adhesion strength, measurements are averaged for powder with an equivalent powder diameter between 20 and 40 μm given an average powder size of 29 μm.

LOM images of failed interfaces were used to investigate the percentage of Ti remaining on the substrate with respect to the projected area of the splat. The area of the remaining Ti on the substrate was measured using color thresholding in ImageJ. The failed interfaces following splat adhesion testing were also analysed using the variable pressure mode of the SEM (SU-3500,

Hitachi, Tokyo, Japan) at an accelerating voltage of 5 kV and a 40 Pa air pressure to reduce charging effects from the bulk ceramic substrate. Metal/ceramic interfaces were cross-sectioned by mechanical grinding and polishing with 0.05 μm colloidal silica mixed with 30 % hydrogen peroxide. Polished interfaces were sputter-coated with chromium to reduce charging effects in the high pressure SEMs (SU-8000, Hitachi, Tokyo). The low accelerating voltage of 5 kV was maintained.

3. Results

3.1 Characterization of Ceramic Substrates

Through EDS analysis, traces of elemental contaminants were found at the surface of both substrates. For Al_2O_3, the contaminants were mainly found between grains (Fig. 2 (a)). The main elements detected were calcium and magnesium with traces of chlorine, sodium and sulfur. These surface contaminants do not seem to influence the results, as backscattered electron (BSE) splat/substrate cross-sectional images do not show changes in contrast near the interface. Therefore, no contaminants are found in the interfaces. Figure 2 (b) shows grains with a dark contrast distributed throughout the surface of the SiC. EDS results showed that these darker grains contained boron. Furthermore, areas with a higher concentration of carbon were observed. Free carbon and boron are used as sintering aids for SiC to improve densification (Ref 31).

The average R_{pk} values of each sample are shown in Fig. 4 (a) for two magnifications. For all samples, the standard deviation is larger when measured at a higher magnification. Positioning of grains and pores does not significantly influence roughness at lower magnifications. Higher magnification measurements on a 87x87 μm^2 surface area are indicative of the local heterogeneity encountered by splats. High standard deviations in surface roughness measurements may be

reflected in variability found in the splat adhesion tests. Single splats encounter various substrate morphologies. Figure 4 (b)-(e) show representative surface topographies of each substrate on a 87x87 μm^2 surface area. The as-received substrates are characterised by a series of fine peaks and valleys due to the morphology of the sintered grains. Polished substrates show minimal fine peaks with valleys caused by porosity.

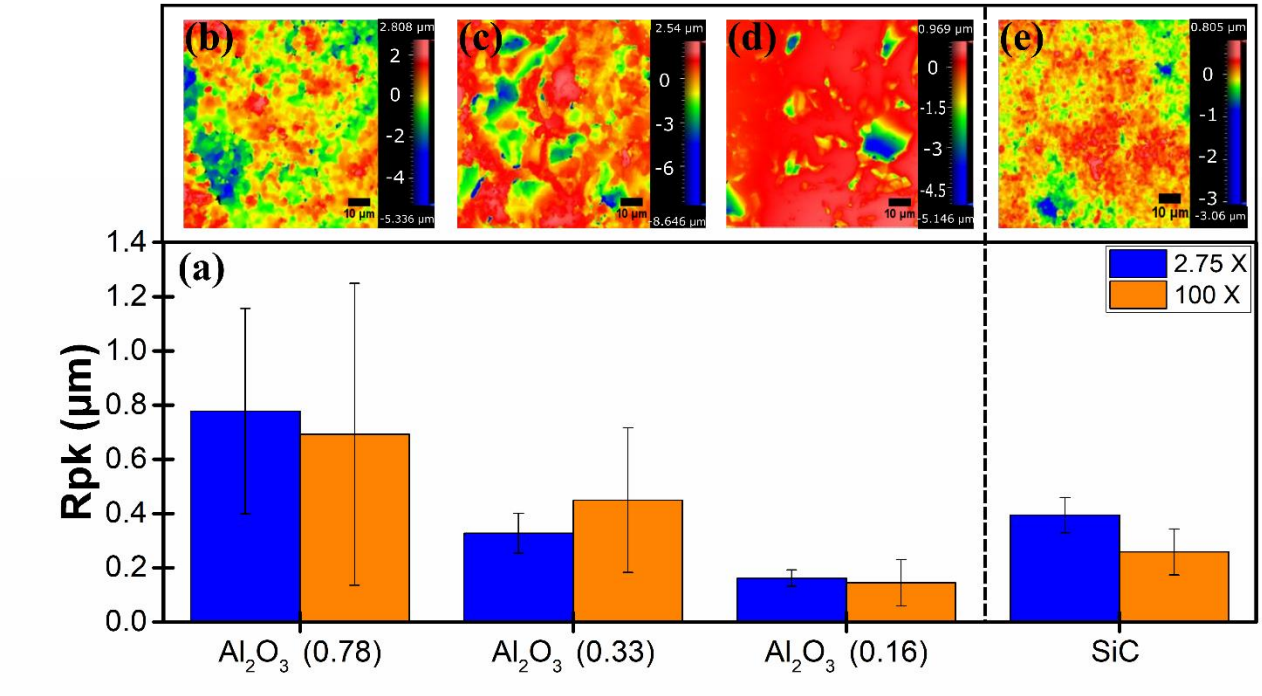

Fig. 4 (a) Surface roughness of Al_2O_3 and SiC substrates in addition to the surface morphology of (b) Al_2O_3 (0.78), (c) Al_2O_3 (0.33) and (d) Al_2O_3 (0.16) and (e) SiC

3.2 Splat Adhesion Testing

3.2.1 Adhesion Strength

Splats with an equivalent powder diameter between 10 μm and 40 um were tested by splat adhesion testing (Fig. 5). For the Al_2O_3 substrates there is a decrease in bond strength with increase in powder diameter (Fig. 5). Similar trends were observed for splat adhesion testing of Ti splats

deposited on Ti substrates (Ref 28). Finer powder particles have higher impact velocities than larger powder particles. The higher impact velocities cause higher adhesion strengths (Ref 28, 32, 33). For the SiC substrate, there are 18 splats that resulted in no distinguishable peak. The adhesion strength for these cases was assumed to be zero. From Fig. 5 (d) null results for the Ti/SiC interface were seen throughout the size distribution. No particular trend or relationship between powder size and probability of a null result was observed for the Ti/SiC interface. For measurable adhesion strengths in the Ti/SiC interface, average adhesion strength appears to be slightly higher than for finer powder particles in the range of 10 to 20 μm. However, there was no trend of adhesion strength with powder diameter for the Ti/SiC interfaces, which was different from the Ti/Al_2O_3 interfaces.

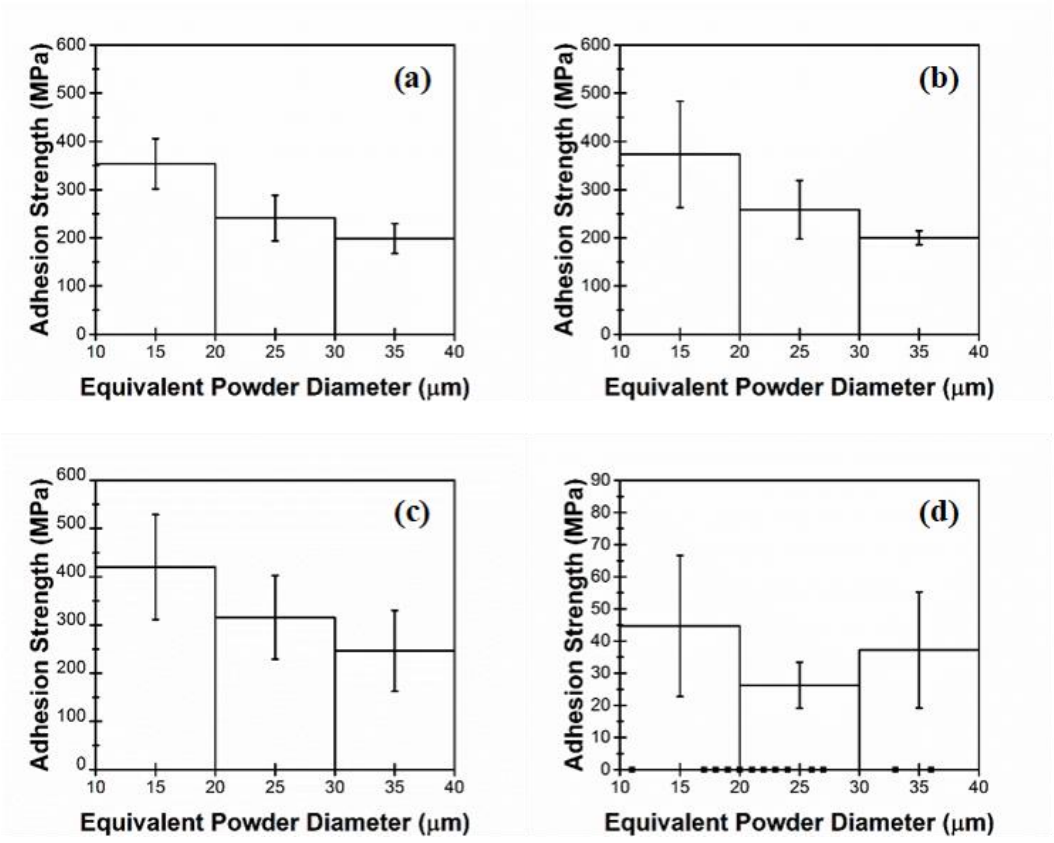

Fig. 5 Effect of equivalent powder diameter on adhesion strength between Ti and (a) Al_2O_3 (0.78), (b) Al_2O_3 (0.33), (c) Al_2O_3 (0.16) and (d) SiC. (d) includes null results for the Ti/SiC interface as points along the x-axis

Given the average powder size of 29 μm and the powder size distribution, averages are compared for an equivalent powder diameter between 20 and 40 μm (Fig. 6). Splat adhesion test results showed significantly higher adhesion between all Ti and Al_2O_3 substrates than between Ti and SiC substrates. 13 of the 26 tests conducted for the Ti/SiC interface, in this size range, resulted in a null adhesion strength. These results were not included to measure the average adhesion strength.

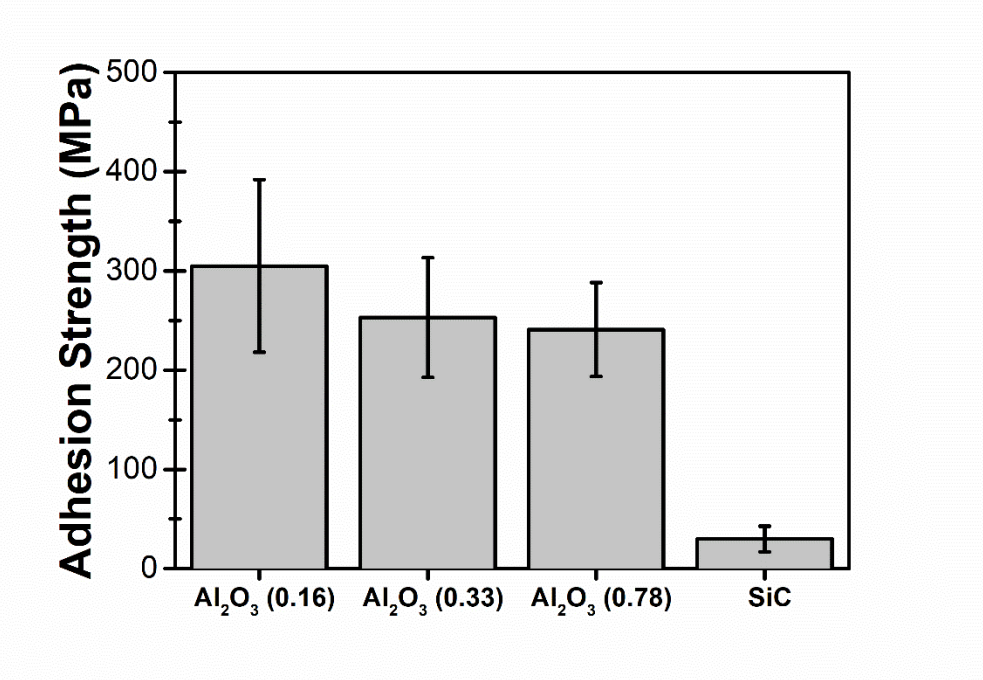

Fig. 6 Average adhesion strength by splat adhesion testing for powder diameters varying from 20 μm to 40 μm deposited on all substrates with the standard deviation as the error bar

Al_2O_3 (0.16) had the highest bond strength. A Student T-test* was used to validate if the bond strength measurements are significantly different with decreasing surface roughness. The difference between Al_2O_3 (0.33) and Al_2O_3 (0.78) was not significant. The difference between Al_2O_3 (0.16) and the two other substrates was significant.

3.2.2 Splat Morphology

Figure 7 shows the top view of a single splat deposited on Al_2O_3 (0.78), Al_2O_3 (0.16) and SiC. Splats typically show jetting along the edges of the powder due to ASI as commonly observed in cold spray (Ref 3, 5). Losses in kinetic energy required to adapt to the rougher substrate morphology do not cause reduced jetting in the Ti/Al_2O_3 interface (Fig. 7 (a)). Also, differences in adhesion strength cannot be identified through splat morphology. Single Ti splats deposited on SiC also show a similar morphology to those deposited on Al_2O_3, despite their significantly lower adhesion strength (Fig. 7 (c)).

* A two-tailed T-test was used given that the number of tests and the variance for each test conditions was not equal. The null hypothesis, that is the hypothesis that there is no difference between the means, was rejected if the P-value was smaller than 0.05. Therefore, a statement can be made that, despite the standard deviation in the data, the means are statistically different with at least a 95 % level of confidence when the null hypothesis is rejected.

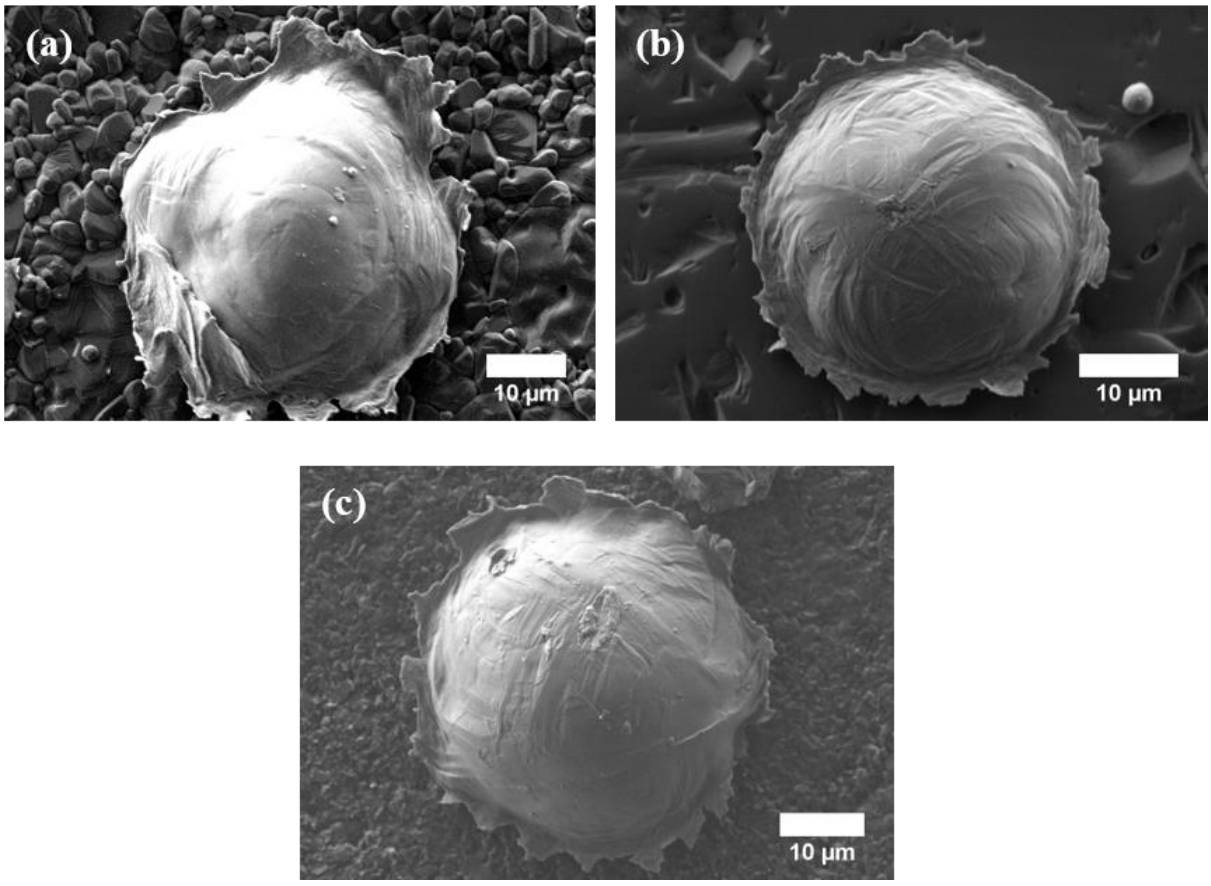

Fig. 7 Single Ti splat deposited on (a) Al_2O_3 (0.78), (b) Al_2O_3 (0.16) and (c) SiC showing formation of ASI

Cross-sectional images of single Ti splats deposited on Al_2O_3 (0.78) (Fig. 8) and SiC (Fig. 9) showed significant differences despite no observable differences in the plan view splat morphology. Cross-sectional imaging of the Ti splats deposited on Al_2O_3 (0.78) showed a very continuous interface. The Ti was found to follow the morphology of the substrate even within pores. Figure 8 (a) shows the interface morphology and Fig. 8 (b) emphasized the grains of the Ti powder through ECC. The material which has penetrated within the pores has nano-sized grains showing evidence of extensive deformation. When the rougher ceramic surface is impacted, the fine peaks create a zone of higher pressure due to the reduced surface area at the location of initial

impact giving localized plasticity within the impacting powder. When the Ti particle impacts on the rougher Al_2O_3 substrate, it is locally deformed around the peaks of the surface, allowing it to penetrate more easily into the pores in addition to the general adiabatic shearing of the particle (Ref 34).

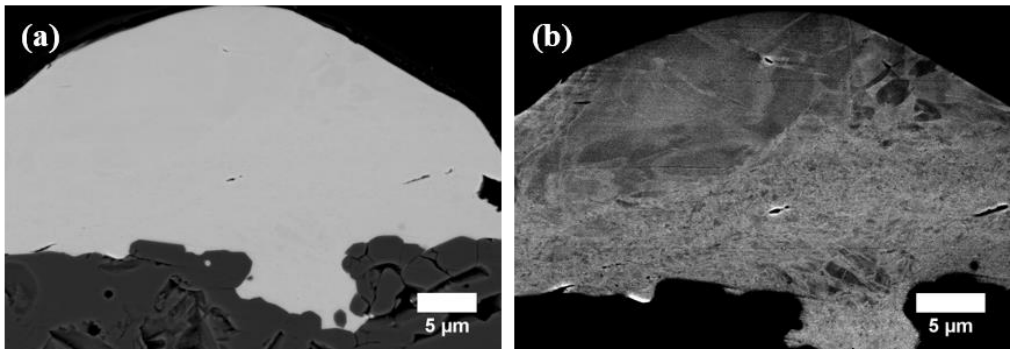

Fig. 8 Backscattered electron microscopy image of single splat cross-section deposited on Al_2O_3 (0.78) emphasizing (a) interface morphology and (b) grain in the Ti splat

Mechanical cross-sectioning of single splats on SiC (Fig. 9) mainly showed gapping between the splat and the substrate with minor mechanical clamping. The weakly bonded particles allowed the epoxy to penetrate the gap between the splat and the substrate (Fig. 9 (a)). The SiC beneath the splat, in some cases, is more porous than the bulk portion (Fig. 9 (b)). Microcracking from the impact occurs in this region. The higher hardness of the SiC makes it more brittle than the Al_2O_3. These microcracks cause material beneath the splat to fall during polishing making it appear more porous.

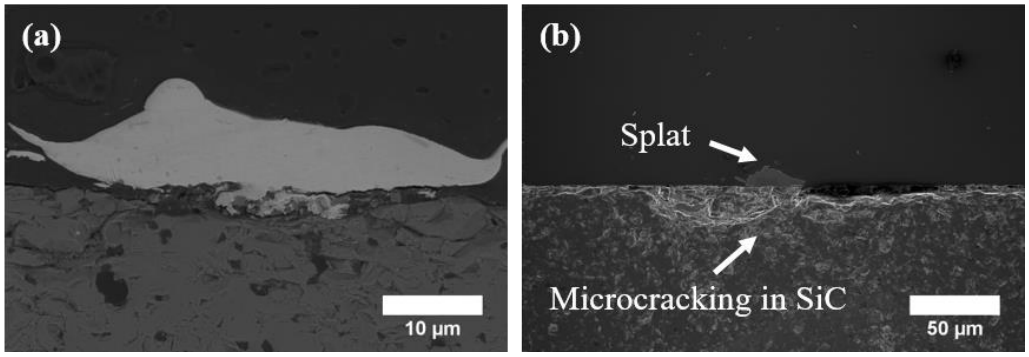

Fig. 9 Cross-section of Ti/SiC interface showing poor bonding. (a) shows a high magnification image to identify interface feature while (b) shows a low magnification image to show cracking in the ceramic substrate

3.2.3 Post-Test Characterization

Failed interfaces from splat adhesion testing revealed traces of Ti on the substrates. The morphology and quantity of the Ti in the failed interface is indicative of the splat's bonding mechanism and strength. Color thresholding of LOM images of the failed interfaces was used to determine the relationship between the amount of Ti on the surface and adhesion strength.

For the Ti/Al_2O_3 (0.16) interface, three cases were observable in post-test characterization. Case 1 is characterized by a circular ring of Ti remaining in the failed interface. The adhering ring of Ti does not significantly protrude from the surface of the substrate. Splats which left a ring on the surface of Al_2O_3 (0.16) impacted areas with minimal porosity. Figure 10 shows a representative image of a Case 1 failed interface. Figure 10 also shows the linear relation with a coefficient of determination (R^2) of 0.8 between the adhesion strength and the percentage of Ti remaining on the substrate for Case 1.

The surface morphology at the splat level can vary significantly even on the polished substrate due to porosity. Pre-existing porosity in the ceramic substrate or potential induced fracture influenced the morphology of the failed interface. In the presence of large pores, the remaining Ti was found

mainly in smooth areas. Figure 10 shows a representative image of a failed interface of this type, which is designated Case 2. Also, a linear relation between adhesion strength and the amount of Ti in the failed interface was found for Case 2 where fit showed an R^2 value of 0.7. The adhesion strength is influenced by removal of Ti from the pore, potential removal of fractured ceramic and shearing of the Ti. For the same percentage of Ti on the substrate, the adhesion strength is higher for Case 2 than Case 1. In Case 1, the shearing of Ti mainly contributes to adhesion strength.

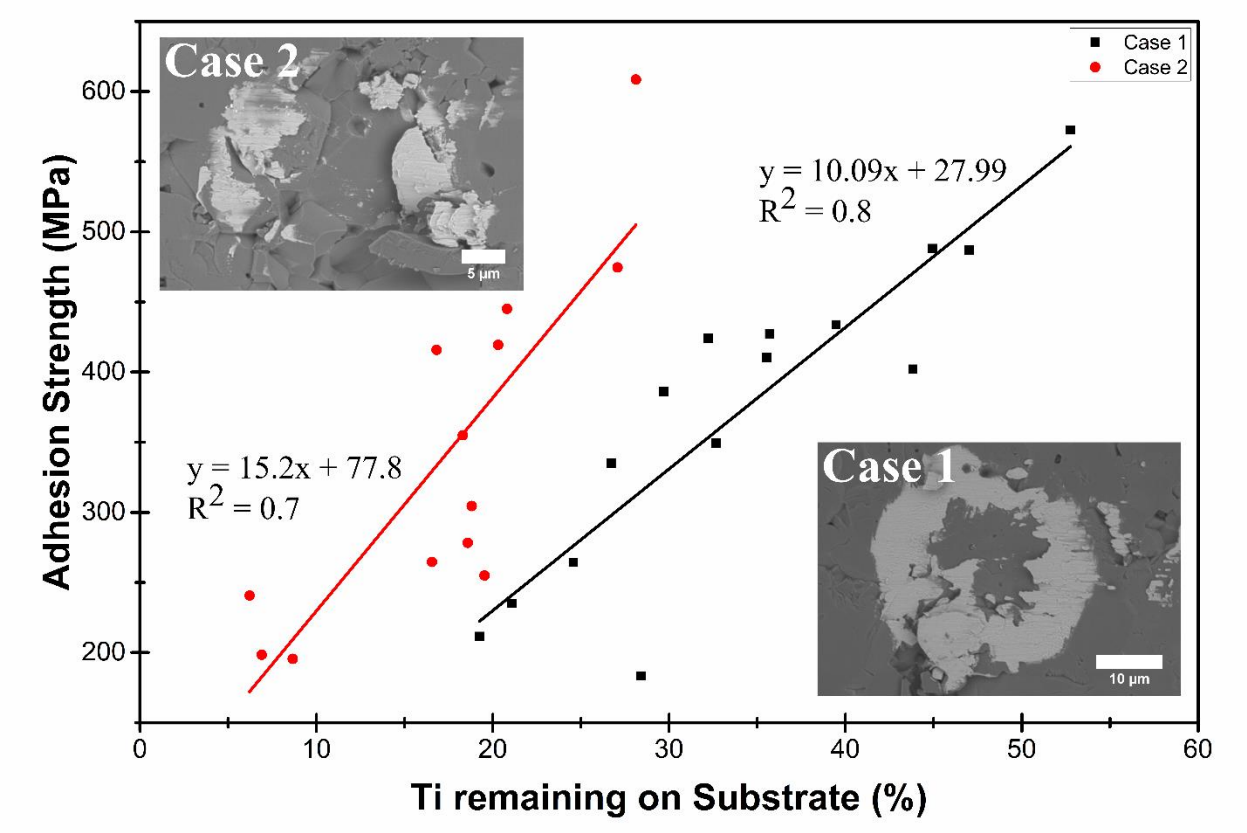

Fig. 10 Adhesion strength with respect to the percentage of Ti remaining on the substrate following splat adhesion testing with regards to the projected splat area for Cases 1 and 2 on Al_2O_3 (0.16). Representative images of Case 1 and Case 2 failed interfaces on Al_2O_3 (0.16) are also included

Case 3 is characterized by a series of fine pores on the surface of Al_2O_3 (0.16). Fine, weakly bonded debris of Ti was found to remain on the substrate following splat adhesion testing (Fig. 11). Only a few tested particles resulted in a Case 3 failed interface. Splats had both high and low adhesion strengths in Case 3. No relationship could be established between percentage of Ti on the substrate and adhesion strength.

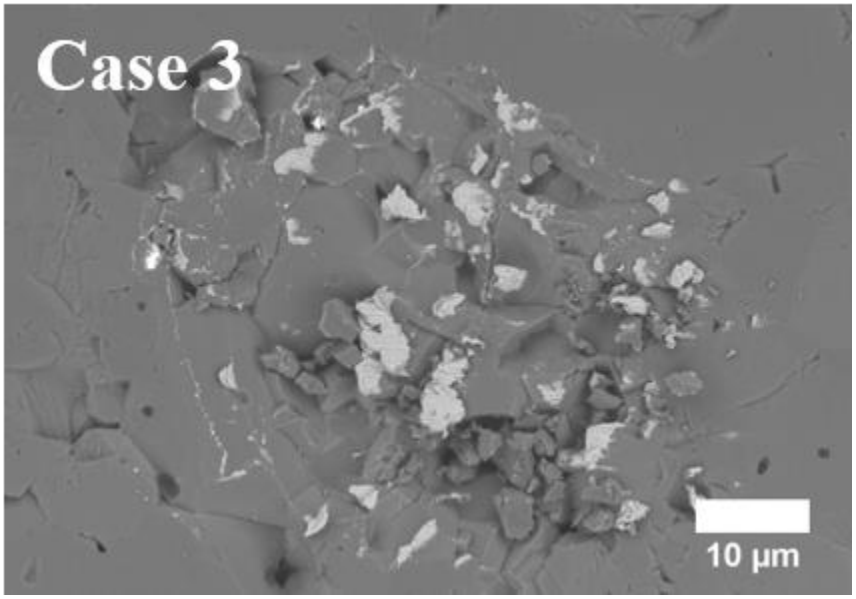

Fig. 11 Case 3 failed interface between Ti on Al2O3 (0.16) following splat adhesion testing

The amount and characteristics of the remaining Ti on the surface of Al_2O_3 (0.33) and Al_2O_3 (0.78) were similar. Scattered parts of Ti remained on the substrates where the splat was removed, showing evidence of localized bonding. Representative images are shown in Fig. 12. Ti remaining on Al_2O_3 (0.78) is mainly within the pores and rarely along the surface of the substrate. These failed interfaces differ from those in Case 3 on Al_2O_3 (0.16) as the Ti remaining on the surface appears well bonded and continuous with the grains of the substrate. From the post-test

characterization, it can be concluded that adhesion strength between single splats of Ti on Al_2O_3 (0.78) is mainly due to mechanical clamping.

The amount of Ti remaining on the substrate varies significantly from one splat to the other. The adhesion strength with respect to the percentage of the Ti remaining on the Al_2O_3 (0.78) substrate was also plotted in Fig. 12. It was found that a linear trend with high variance ($R^2 = 0.45$) exists between adhesion strength and quantity of Ti remaining on the substrate. Similarly to Case 2 on the Al_2O_3 (0.16) substrate, the high variance can be attributed to effects contributing to adhesion strength measurements such as the extraction of Ti from within pores or detachment of ceramic grains. The adhesion strength for low percentages of Ti on the substrate is higher than what was observed for the Al_2O_3 (0.16) substrate. However, the splats deposited on Al_2O_3 (0.16) tend to have a higher percentage of Ti remaining on the substrate, following the test, contributing to its overall higher average adhesion.

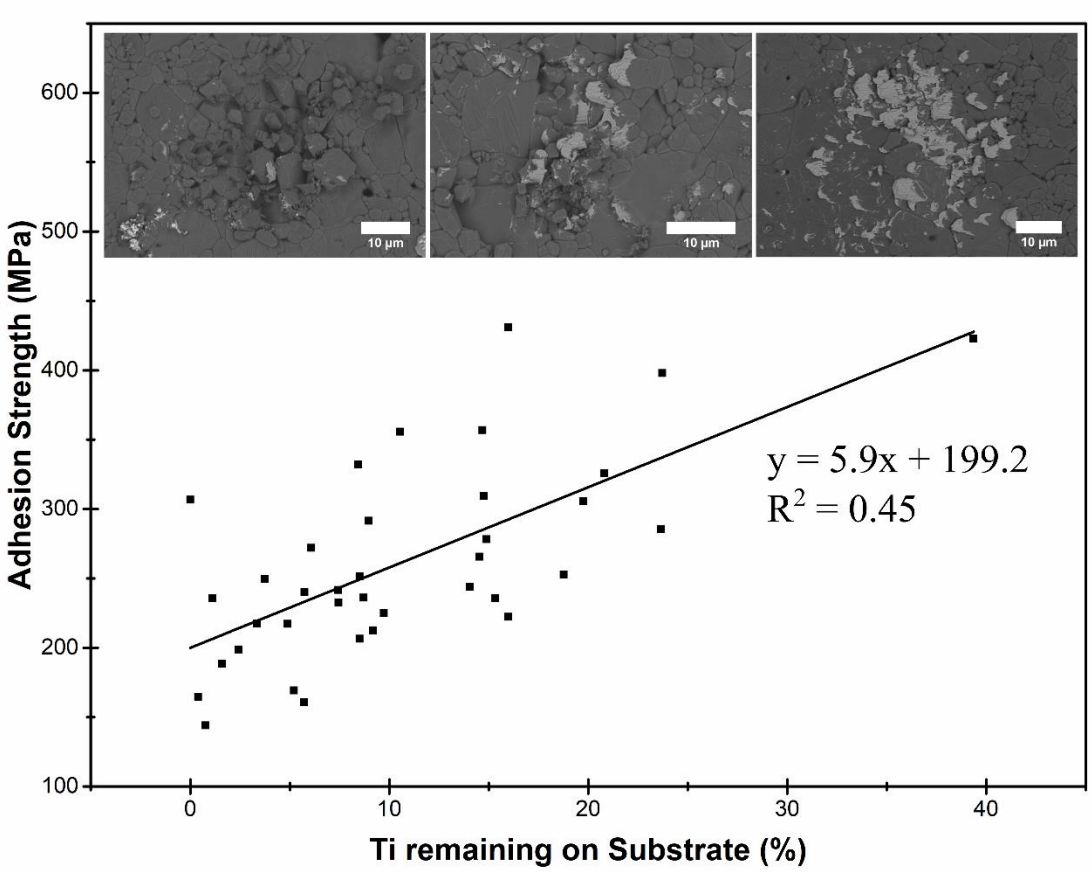

Fig. 12 Adhesion strength with respect to the amount of Ti that remains on the substrate following splat adhesion testing for the Al_2O_3 (0.78) substrate

The bonding mechanism of Ti particles sprayed on smooth and rough Al_2O_3 substrates is significantly different. Mechanical clamping appears to play a more significant role in bonding with the rougher surfaces, but mechanical clamping is not necessarily the only bonding mechanism for cold spraying metal powder on ceramic substrates given the results obtained on the smoother substrates. Bonding also occurs in the zone of ASI, where the temperature is at the highest and deformation is most significant (Ref 3, 35). Hence, ASI is likely a necessary occurrence for bonding on the smooth ceramic substrates.

For the Ti splats deposited on SiC, following splat adhesion testing, there is mainly no evidence of bonding with no Ti remaining on the substrate. Fracture of the substrate is sometimes observable or, in very few cases, a small portion of Ti remained on the substrate (Fig. 13).

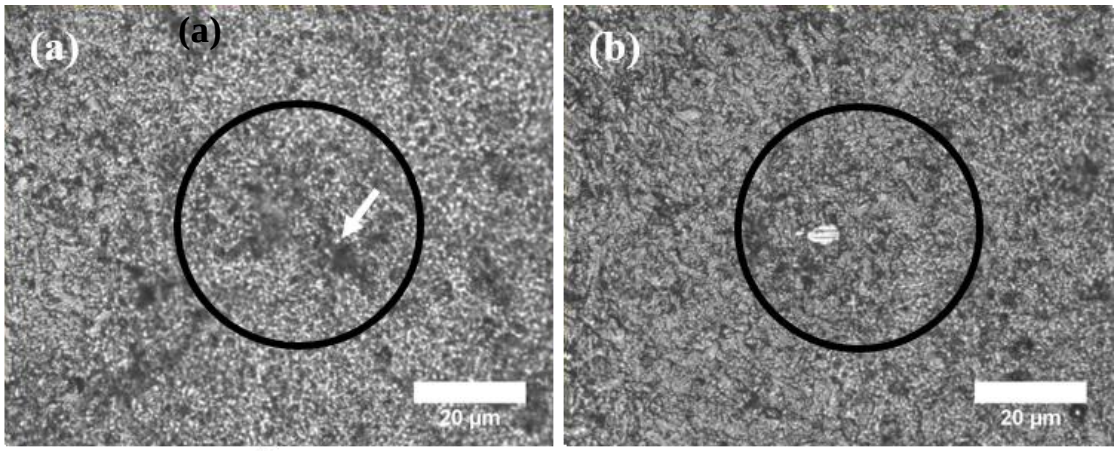

Fig. 13 Representative LOM image of failed interface on SiC (a) shows a remaining interface with no evidence of Ti and some minor fracturing of the ceramic identified by an arrow, and (b) shows minor evidence of Ti remaining on the SiC

BSE images revealed traces of Ti on the surface of the substrate from rebounded or weakly bonded particles which fell off of the substrate. A splat that was removed by splat adhesion testing could not be distinguished from a rebounded splat. These fine traces of Ti were not identifiable by LOM. The traces of Ti remaining on the substrate due to rebounded or detached splats are in the shape of a ring (Fig. 14). Within the ring, the fine traces of Ti appear along the surface and not solely within cracks. This demonstrates that extremely localized bonds are formed within the same area that a complete bond is formed between some Ti splats and Al_2O_3 (0.16) substrate. An example is marked by an arrow in Fig. 14. Bonding between Ti and SiC is extremely localized in comparison to Al_2O_3.

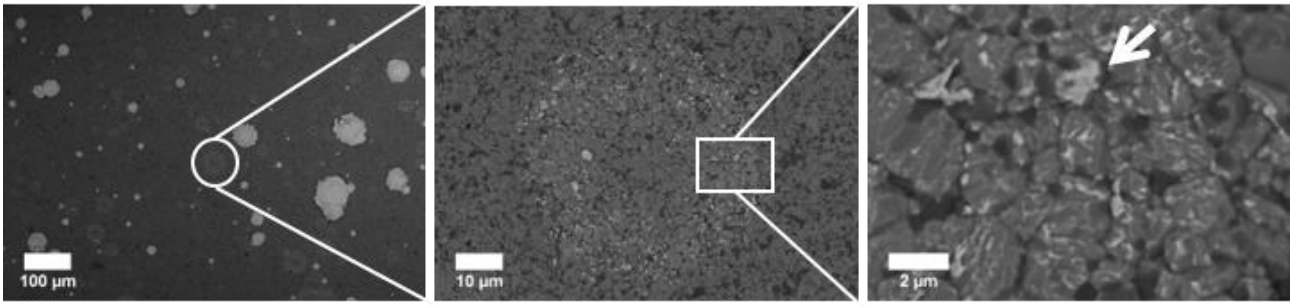

Fig. 14 Circular ring with traces of Ti appearing on SiC in locations where the particle has rebounded or fallen

4. Discussion

4.1 Adhesion strength

Direct comparisons of splat adhesion test to a bulk coating adhesion test are somewhat difficult due to the different length scales and different loading conditions. Splat adhesion test data provides adhesion at the single splat level while typical tensile testing techniques are intended to characterize full coatings. Goldbaum et al. (Ref 28) showed however that splat adhesion tests correlated well to a bulk coating cohesion measurement for cold sprayed Ti. For the Ti/Al_2O_3 and Ti/SiC systems, this work represents the first application of the splat adhesion test. Also, even for bulk tests, there have been no reported bond strength measurements for the Ti/Al_2O_3 and Ti/SiC interface in previous literature. However, some qualitative comparisons can be made using other material systems. Few metal coatings deposited on ceramic substrates by cold spray have been tested by bulk coating adhesion tests. Al has been the most prominent metal investigated in metal/ceramic adhesion by cold spray. Adhesion of Al coatings to MgF_2, Al_2O_3, Si_3N_4, SiC and AlN substrates maintained at room temperature are all significantly lower than values obtained here in the Ti/Al_2O_3 interface (Ref 18, 19, 21, 22). Higher adhesion strengths are obtained with an increase in substrate temperature and through heat treatment (Ref 18, 22). Values remain lower than

adhesion between Ti and Al_2O_3. Bulk coating adhesion tests of Al/SiC interfaces are comparable to values obtained by splat adhesion testing in the Ti/SiC interface.

The bond strength of Ti deposited on Al_2O_3 is comparable or, in some cases, higher than the values reported by Goldbaum et al. for Ti deposited on Ti (Ref 28). The sheared Ti remaining in the failed interface has been highly deformed at impact, and therefore has a higher shear strength than bulk Ti. The Al_2O_3 substrate has a higher hardness than a Ti substrate. Thus, the impact onto Al_2O_3 induces more deformation in the splat than the Ti substrate at impact. This phenomenon can explain the higher adhesion strength measured in certain cases in the Ti/Al_2O_3 interface. Removal of fractured ceramic grains or surface roughness can also influence adhesion in the Ti/Al_2O_3 interface.

For metal/metal splat adhesion testing, where the two metals are of the same material, it is impossible to determine the fraction of metal from the splat remaining on the substrate. However, in the work of Goldbaum et al., they observed that, for their highest adhesion strengths, the test was shearing through the splat very close to the bonded interface (Ref 28). This indicates a very good metallurgical bond and the splat adhesion test at this point measures mechanical properties of the splat itself. From post-test characterization of Ti/Al_2O_3 interfaces, the amount of Ti remaining on the substrate was measured and correlated to the bond strength. Also, the morphology of the remaining Ti provided information with regards to the bonding mechanism. As the tip applies a tangential pressure on the splat, an interface crack spreads leading to the eventual detachment of the splat. The crack spreads through the weakest part of the interface. In the case where crack spreading leaves Ti on the surface of the substrate, it is indicative of a strong bond between the splat and the substrate. The adhesion at the interface is stronger than the cohesion of the splat itself. This was observed when Ti was deposited on Al_2O_3 (0.16). When deposited on

Al_2O_3 (0.78), the Ti remained within pores rather than on the surface. The interface was therefore composed of both Al_2O_3 and Ti. When mechanical bonding is the predominant bonding mechanism, shearing of Ti is necessary to remove the splat. Splat adhesion testing in the rough interface therefore provides a measure of how well the particle is mechanically bonded.

4.2 Adhesion Rings

Adhesion between single splats of Ti and smooth substrates was not solely dependent on mechanical clamping. Following splat adhesion testing, a ring of Ti remained on Al_2O_3 (0.16) in locations where minimal porosity was observed. Similarly, fine traces of Ti were found in a ring shape when deposited on SiC for rebounded or fallen splats. Various models (Ref 3, 5, 35) and experimental works (Ref 28, 36) have shown the link between ASI and adhesion in metallic systems. In splat adhesion testing, a similar ring was previously observed for Ti/Ti and Ti6Al4V/Ti6Al4V interfaces as reported by Goldbaum et al. (Ref 28). While the center of the powder is exposed to the highest hydrostatic pressure, adhesion does not occur. Rather, shear forces within the adiabatically sheared jet are associated with bonding (Ref 8, 23, 36, 37). The presence of a ring of Ti on Al_2O_3 (0.16) and on SiC shows that ASI are significant to bonding in metal/ceramic systems with low surface roughness. Adhesion in the periphery of single splats of Ti deposited onto ZrO_2 due to ASI has also previously been shown (Ref 23). Similarly, adhesion rings were observed for Cu/Al_2O_3 interfaces (Ref 11).

Drehmann et al. (Ref 18, 19), as well as Wüstefeld et al. (Ref 13) and Rafaja et al. (Ref 17) also suggested that mechanical clamping is not the sole contributing factor to adhesion in metal/ceramic interfaces created by cold spray. Hetero-epitaxy between the metal and ceramic lattices contributes to bonding due to the energy stored in microstructural defects caused during plastic deformation

in the metal and heating in the interface (Ref 13, 17, 18, 19). Rafaja et al. extended the concept of hetero-epitaxy to polycrystalline Al_2O_3 interfacing Ti, as these materials show a small lattice misfit along multiple planes (Ref 17). On the other hand, Ko et al. attributed adhesion in metal/ceramic systems to atomic intermixing as a result of amorphisation due to extreme plastic deformation (Ref 20). Also, Kim et al. suggested that bonding is attributable to the intimate contact between the metal and the ceramic as surface oxides are removed due to ASI (Ref 23). Surface activated bonding is based on the premise that two clean surfaces in intimate contact will form a bond. Clean metal surfaces have a natural tendency to react with oxygen, nitrogen or carbon (Ref 38, 39). Metals and oxides have been shown to bond by this technique in their solid-state (Ref 23, 39). Here, it was shown that adhesion occurs due to ASI in smooth interfaces. ASI are associated to the location of highest temperature. The previously discussed bonding mechanisms such as hetero-epitaxy, surface activated bonding or atomic intermixing due to amorphisation require atomic motion at the interface. It is therefore consistent that ASI lead to the formation of any of these chemico-physical interactions.

4.3 Effect of surface roughness

From post-test characterization of single splats deposited on Al_2O_3 with different surface roughness, mechanical clamping is observed when peaks and valleys are present. On the rougher substrate, Ti remained between the grains of Al_2O_3 but for splats on smoother surfaces, a ring morphology was observed showing evidence of a potential chemical interaction. There are only few studies addressing surface roughness in metal/ceramic interfaces created by cold spray. Images of Al splats deposited on Al_2O_3 revealed that mechanical bonding assisted in bond formation on rougher substrate or though porosity on smoother substrates (Ref 19). However, a Ti coating on a smooth sapphire substrate was well-bonded while deposition onto a rougher sapphire substrate resulted in delamination (Ref 17).

Some insight can also be obtained from the literature on metal/metal interfaces. Hussain et al. observed that high surface roughness prevented metallurgical bonding in an Al/Cu interface. Mechanical bonding was the main bonding mechanism (Ref 40). Kumar et al. also found that when depositing a soft metal on a hard metal (Al on mild steel), surface roughness influenced adhesion. The bond strength increased with surface roughness until a certain point. For very rough substrates, adhesion decreased. Mixed adhesion mechanisms (metallurgical bonding and mechanical bonding) allowed for high adhesion strength in intermediate surface roughness values (Ref 41). Similarly in this work, roughness highly influenced the adhesion mechanism in the Ti/Al_2O_3 interface. A transition from mechanical bonding to chemical bonding was observable with decreased surface roughness.

4.4 Effect of substrate composition

Drehmann et al. (Ref 18) investigated the effect of the percentage of ionic and covalent bonding in the ceramic on adhesion between the Al and various ceramics in cold spray, as more covalently bonded ceramics tend to be easily wetted by metals. However, higher ionicity of the ceramic did not correlate to higher adhesion strength. Furthermore, poor bonding was not adequately explained by differences in coefficients of thermal expansion mismatch between the metal and the ceramic. Instead, they proposed that a ceramic's higher thermal conductivity can assist in the formation of a hetero-epitaxial bond (Ref 18). For the Ti splats interfacing with Al_2O_3 and SiC, a stronger bond was formed with the more ionic ceramic further emphasizing that the bond between the cold sprayed metal and the ceramic does not follow the same trend as wetting behaviours between them. From the manufacturer data sheet, Al_2O_3 has a thermal conductivity of 30 W/mK and SiC 150 W/mK. The higher thermal conductivity of the SiC did not assist in the formation of a bond. Ti splats deposited on SiC appear to form highly localized, weak bonds. Gaps were found through most of the interface of the deposited single splats. Drehmann et al. also observed significant gapping between a full coating of Al on SiC and single Al splats on Al_2O_3 substrate (Ref 18, 19). This is considerably different to what was observed when depositing single Ti splats on Al_2O_3. The Ti/Al_2O_3 interface appeared continuous and rendered very strong bonds under identical spray conditions to the depostion of Ti on SiC. Cracking of SiC was observed for Ti/SiC interfaces. This shows that the impact fracture toughness of the ceramic influences adhesion in cold sprayed metal/ceramic interfaces.

5. Conclusion

A better understanding of metal/ceramic interfaces is necessary to optimize metal matrix composites and ceramic metallization created by cold spray. Splat adhesion testing provided insight into bond formation between Ti splats deposited on Al_2O_3 and SiC. The adhesion strength of Ti deposited on Al_2O_3 is shown to be significantly higher than SiC. The type of ceramic has an important influence on adhesion. The Ti/SiC interface showed micro-cracking of the ceramic and gapping while the Ti/Al_2O_3 interface appeared continuous.

The as-received ceramic substrates had significantly different roughness. Al_2O_3 was therefore polished to three final roughnesses of R_{pk} = 0.78, 0.33 and 0.16 µm to investigate the effect of surface roughness on adhesion strength. The bonding mechanism between Al_2O_3 (0.78) and Al_2O_3 (0.16) was significantly different. Splats deposited on Al_2O_3 (0.78) bonded mechanically with Ti infiltration into surface pores. Splats deposited on non-porous sections of Al_2O_3 (0.16) formed adhesion rings due to ASI. Where large pores on Al_2O_3 (0.16) were present, Ti remained on the substrate in the comparatively smooth areas. Some splats landed in areas with fine pores and left minimal Ti on the surface. For the same amount of Ti remaining in the failed interface, splats landing in large pores had higher adhesion strength given influencing factors such as pull out of ceramic grains or Ti from the pores. The amount of Ti remaining on the substrate following splat adhesion testing influences adhesion strength on all Al_2O_3 substrates.

The failed Ti/SiC interface showed very little evidence of bonding in localized areas. A significant amount of Ti powder rebounded from the substrate leaving rings with fine traces of Ti on the SiC substrate. No traces of rebound were observed on Al_2O_3 substrates. While ASI led to a continuous ring of Ti for many splats on Al_2O_3 (0.16), it led to weak localized bonds in the Ti/SiC interface.

Acknowledgments The authors gratefully acknowledge the assistance of Dr. Phuong Vo and Jean-Francois Alarie at the McGill Aerospace Materials and Alloys Design Center (MAMADC) for technical support with the cold spray equipment. They also, thank Thomas Schmitt and Jolanta Sapieha for technical support and access to the scratch tester. This project would also not have been possible without the financial support from the Natural Science and Engineering Research Council (NSERC) Strategic Grants Program.

References

1. A. Papyrin, *Cold Spray Technology*. Elsevier, Amsterdam, The Netherlands, 2007.
2. J. Villafuerte, *Modern Cold Spray : Materials, Process, and Applications*. Springer, Windsor, Ontario, Canada, 2015.
3. H. Assadi, F. Gärtner, T. Stoltenhoff, and H. Kreye, Bonding Mechanism in Cold Gas Spraying, *Acta Mater.*, 2003, **51**(15), p 4379-4394
4. H. Assadi, T. Schmidt, H. Richter, J. O. Kliemann, K. Binder, F. Gärtner, T. Klassen, and H. Kreye, On Parameter Selection in Cold Spraying, *J. Therm. Spray Technol.*, 2011, **20**(6), p 1161-1176
5. M. Grujicic, C. L. Zhao, W. S. De Rosset, and D. Helfritch, Adiabatic Shear Instability Based Mechanism for Particles/Substrate Bonding in the Cold-Gas Dynamic-Spray Process, *Mater. Des.*, 2004, **25**(8), p 681-688
6. A. Moridi, S. M. Hassani-Gangaraj, M. Guagliano, and M. Dao, Cold Spray Coating: Review of Material Systems and Future Perspectives, *Surf. Eng.*, 2014, **30**(6), p 369-395
7. H. Y. Lee, Y. H. Yu, Y. C. Lee, Y. P. Hong, and K. H. Ko, Cold Spray of Sic and Al2o3 with Soft Metal Incorporation: A Technical Contribution, *J. Therm. Spray Technol.*, 2004, **13**(2), p 184-189
8. H. Assadi, H. Kreye, F. Gärtner, and T. Klassen, Cold Spraying - a Materials Perspective, *Acta Mater.*, 2016, **116**, p 382-407
9. R. R. Chromik, S. A. Alidokht, J. M. Shockley, and Y. Zhang, Tribological Coatings Prepared by Cold Spray, *Cold-Spray Coatings: Recent Trends and Future Perspectives*. P. Cavaliere, Springer International Publishing, Cham, Switzerland, 2018, p 321-348
10. K.-R. Donner, F. Gaertner, and T. Klassen, Metallization of Thin Al2o3 Layers in Power Electronics Using Cold Gas Spraying, *J. Therm. Spray Technol.*, 2011, **20**(1-2), p 299-306
11. K. R. Ernst, J. Braeutigam, F. Gaertner, and T. Klassen, Effect of Substrate Temperature on Cold-Gas-Sprayed Coatings on Ceramic Substrates, *J. Therm. Spray Technol.*, 2013, **22**(2-3), p 422-432
12. B. Wielage, T. Grund, C. Rupprecht, and S. Kuemmel, New Method for Producing Power Electronic Circuit Boards by Cold-Gas Spraying and Investigation of Adhesion Mechanisms, *Surf. Coat. Technol.*, 2010, **205**(4), p 1115-1118
13. C. Wüstefeld, D. Rafaja, M. Motylenko, C. Ullrich, R. Drehmann, T. Grund, T. Lampke, and B. Wielage, Local Heteroepitaxy as an Adhesion Mechanism in Aluminium Coatings Cold Gas Sprayed on Aln Substrates, *Acta Mater.*, 2017, **128**, p 418-427
14. L. L. Hench, and S. M. Best, Ceramics, Glasses, and Glass-Ceramics: Basic Principles, *Biomaterials Science*, 3rd ed., B. D. Ratner, A. S. Hoffman, F. J. Schoen and J. E. Lemons, Academic Press, Kidlington, Oxford, 2013, p 128-151
15. J. B. Brunski, Metals: Basic Principles, *Biomaterials Science*, 3rd ed., B. D. Ratner, A. S. Hoffman, F. J. Schoen and J. E. Lemons, Academic Press, Kidlington, Oxford, 2013, p 111-119
16. H. Lee, and K. Ko, Effect of Sic Particle Size on Cold Sprayed Al-Sic Composite Coatings, *Surf. Eng.*, 2009, **25**(8), p 606-611
17. D. Rafaja, T. Schucknecht, V. Klemm, A. Paul, and H. Berek, Microstructural Characterisation of Titanium Coatings Deposited Using Cold Gas Spraying on Al2o3 Substrates, *Surf. Coat. Technol.*, 2009, **203**(20-21), p 3206-3213

18. R. Drehmann, T. Grund, T. Lampke, B. Wielage, K. Manygoats, T. Schucknecht, and D. Rafaja, Interface Characterization and Bonding Mechanisms of Cold Gas-Sprayed Al Coatings on Ceramic Substrates, *J. Therm. Spray Technol.*, 2015, **24**(1-2), p 92-99
19. R. Drehmann, T. Grund, T. Lampke, B. Wielage, K. Manygoats, T. Schucknecht, and D. Rafaja, Splat Formation and Adhesion Mechanisms of Cold Gas-Sprayed Al Coatings on Al2o3 Substrates, *J. Therm. Spray Technol.*, 2014, **23**(1-2), p 68-75
20. K. H. Ko, J. O. Choi, and H. Lee, The Interfacial Restructuring to Amorphous: A New Adhesion Mechanism of Cold-Sprayed Coatings, *Mater. Lett.*, 2016, **175**, p 13-15
21. S. Kümmel, T. Grund, P. Löschner, and B. Wielage, Influence of Deposition Conditions and Heat Treatment on Tensile Strength of Cold Spray Aluminium Coatings on Al2o3 and Aln Substrates, *Thermal Spray 2011: Proceedings of the International Thermal Spray Conference*, September 26-29, 2011, (Hamburg, Germany), DSV, 2011, p 1130-1135
22. R. Drehmann, T. Grund, T. Lampke, B. Wielage, C. Wüstefeld, M. Motylenko, and D. Rafaja, Essential Factors Influencing the Bonding Strength of Cold-Sprayed Aluminum Coatings on Ceramic Substrates, *J. Therm. Spray Technol.*, 2018, **27**(3), p 446-455
23. K. H. Kim, M. Watanabe, and S. Kuroda, Bonding Mechanisms of Thermally Softened Metallic Powder Particles and Substrates Impacted at High Velocity, *Surf. Coat. Technol.*, 2010, **204**(14), p 2175-2180
24. A. Sova, V. F. Kosarev, A. Papyrin, and I. Smurov, Effect of Ceramic Particle Velocity on Cold Spray Deposition of Metal-Ceramic Coatings, *J. Therm. Spray Technol.*, 2011, **20**(1-2), p 285-291
25. A. Sova, A. Papyrin, and I. Smurov, Influence of Ceramic Powder Size on Process of Cermet Coating Formation by Cold Spray, *J. Therm. Spray Technol.*, 2009, **18**(4), p 633-641
26. S. V. Klinkov, and V. F. Kosarev, Cold Spraying Activation Using an Abrasive Admixture, *J. Therm. Spray Technol.*, 2012, **21**(5), p 1046-1053
27. R. R. Chromik, D. Goldbaum, J. M. Shockley, S. Yue, E. Irissou, J. G. Legoux, and N. X. Randall, Modified Ball Bond Shear Test for Determination of Adhesion Strength of Cold Spray Splats, *Surf. Coat. Technol.*, 2010, **205**(5), p 1409-1414
28. D. Goldbaum, J. M. Shockley, R. R. Chromik, A. Rezaeian, S. Yue, J. G. Legoux, and E. Irissou, The Effect of Deposition Conditions on Adhesion Strength of Ti and Ti6al4v Cold Spray Splats, *J. Therm. Spray Technol.*, 2012, **21**(2), p 288-303
29. "Sintered Metal Materials, Excluding Hardmetals - Measurement of Surface Roughness," ISO 23519:2010, *International Organization for Standardization ISO*, 2010
30. K. Kim, M. Watanabe, and S. Kuroda, Thermal Softening Effect on the Deposition Efficiency and Microstructure of Warm Sprayed Metallic Powder, *Scr. Mater.*, 2009, **60**(8), p 710-713
31. K. Yamada, and M. Mohri, Properties and Applications of Silicon Carbide Ceramics, *Silicon Carbide Ceramics--1 : Fundamental and Solid Reaction*. S. Sömiya and Y. Inomata, Elsevier, London, England, 1991, p 13-44
32. T. Schmidt, F. Gärtner, H. Assadi, and H. Kreye, Development of a Generalized Parameter Window for Cold Spray Deposition, *Acta Mater.*, 2006, **54**(3), p 729-742
33. B. Samareh, and A. Dolatabadi, A Three-Dimensional Analysis of the Cold Spray Process: The Effects of Substrate Location and Shape, *J. Therm. Spray Technol.*, 2007, **16**(5-6), p 634-642
34. T. Hussain, Cold Spraying of Titanium: A Review of Bonding Mechanisms, Microstructure and Properties, *Key Eng. Mater.*, 2013, **533**, p 53-90
35. G. Bae, Y. Xiong, S. Kumar, K. Kang, and C. Lee, General Aspects of Interface Bonding in Kinetic Sprayed Coatings, *Acta Mater.*, 2008, **56**(17), p 4858-4868

36. M. V. Vidaller, A. List, F. Gaertner, T. Klassen, S. Dosta, and J. M. Guilemany, Single Impact Bonding of Cold Sprayed Ti-6al-4v Powders on Different Substrates, *J. Therm. Spray Technol.*, 2015, **24**(4), p 644-658
37. T. Schmidt, F. Gartner, H. Assadi, and H. Kreye, Development of a Generalized Parameter Window for Cold Spray Deposition, *Acta Mater.*, 2006, **54**(3), p 729-742
38. T. Akatsu, N. Hosoda, T. Suga, and M. Rühle, Atomic Structure of Al/Al Interface Formed by Surface Activated Bonding, *J. Mater. Sci.*, 1999, **34**(17), p 4133-4139
39. M. Aghasibeig, H. Monajatizadeh, P. Bocher, A. Dolatabadi, R. Wuthrich, and C. Moreau, Cold Spray as a Novel Method for Development of Nickel Electrode Coatings for Hydrogen Production, *Int. J. Hydrogen Energy*, 2016, **41**(1), p 227-238
40. T. Hussain, D. G. McCartney, P. H. Shipway, and D. Zhang, Bonding Mechanisms in Cold Spraying: The Contributions of Metallurgical and Mechanical Components, *J. Therm. Spray Technol.*, 2009, **18**(3), p 364-379
41. S. Kumar, G. Bae, and C. Lee, Influence of Substrate Roughness on Bonding Mechanism in Cold Spray, *Surf. Coat. Technol.*, 2016, **304**, p 592-605